E-ISSN No : 2456-5040 | Volume : 11 | Issue : 4 | April 2026

HEAT TRANSFER ANALYSIS AND MATHEMATICAL MODELING OF SS304 MATERIAL BY LENS™ TECHNOLOGY

Chirag A. Patel[1], Prof. Dhaval Chauhan[1]

Access Online

Article DOI:
10.5281/zenodo.19968109

[1] Department of Mechanical Engineering, Monark University

How to Cite:
Chirag A. Patel, Prof. Dhaval Chauhan (2026), Heat Transfer Analysis and Mathematical Modeling of SS304 Material By LENS™ Technology, International Educational Applied Scientific & Research Journal (IEASRJ), Vol: 11, Issue: 4, 39-45

ABSTRACT

Laser Engineered Net Shaping ($LENS_U$) is an advanced rapid manufacturing technique that encompasses intricate thermal, mechanical, and metallurgical interactions. The Finite Element Method (FEM) offers a highly accurate framework for simulating this process, thereby enabling the optimized selection of process input parameters and facilitating the production of components with enhanced thermo-mechanical characteristics. In the present investigation, the commercially available FEM software ANSYS is employed to predict transient thermal histories, total structural deformation, von Mises stress distributions, and shear stress fields generated within a thin-walled structure and its supporting substrate, both fabricated from AISI 304 stainless steel. The numerically obtained results are subsequently validated against experimentally measured data to establish the reliability and accuracy of the proposed computational framework.

KEYWORDS: Laser Engineered Net Shaping ($LENS_U$), Finite Element Method (FEM), total Deformation, Von Mises Stress, Shear Stress, Element Birth and Death Technique

1. INTRODUCTION

Laser Engineered Net Shaping ($LENS_U$) is a rapid manufacturing technology originally developed by Sandia National Laboratories (SNL) that synergistically integrates the principles of powder injection and laser welding to achieve the direct fabrication of near-net-shape metallic components. In numerous respects, $LENS_U$ shares operational characteristics with single-step laser cladding. However, while laser cladding is predominantly employed to bond metallic coatings onto the surfaces of pre- manufactured components using conventional processing methods, $LENS_U$ enables the complete fabrication of three- dimensional, fully dense metallic parts through the sequential, layer-by-layer deposition of laser-melted metallic powder.

In this process, a focused laser beam is directed onto the surface of a metallic substrate to generate a localized molten pool. Metallic powder is subsequently propelled by an inert carrier gas — typically argon or nitrogen — through converging nozzles and delivered into the molten pool. Depending on the relative alignment of the nozzle focal point with respect to that of the laser beam, the powder particles are melted either in mid-flight or upon entry into the molten pool. As the laser source traverses away from the

deposition zone, the molten material undergoes rapid solidification through conductive heat dissipation into the substrate, resulting in a consolidated, solid deposit.

The substrate is mounted on a three- or five- axis positioning stage capable of controlled translational motion in the X and Y directions. A three-dimensional CAD model is initially constructed to define the geometry of the desired component. This model is subsequently converted into a faceted representation comprising multiple planar cross-sectional slices, each governing the motion of the X–Y stage and corresponding to a single deposition layer. During fabrication, the integrated powder-nozzle/laser/stage assembly traces a two- dimensional contour of the cross-sectional boundary defined by each slice in the X–Y plane, and subsequently fills the enclosed area according to an operator-specified rastering pattern.

Fig. 1.1 : A schematic diagram of the LENS process[12]

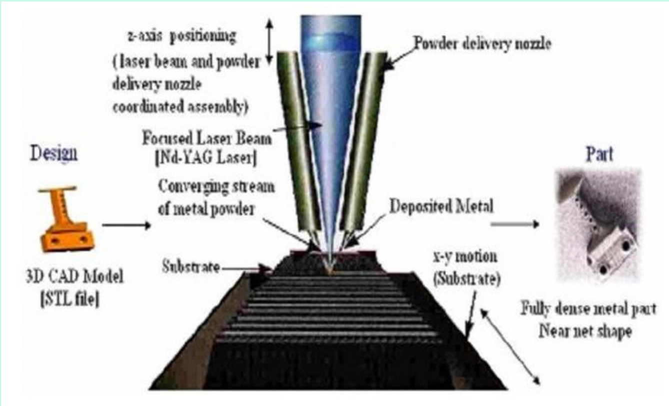

Upon completion of each layer, the laser/nozzle assembly ascends incrementally in the Z-direction to facilitate the deposition of the subsequent layer. This sequence is repeated iteratively for all successive layers until the three-dimensional component is fully constructed.

2. LITERATURE REVIEW

Keicher et al. [5] investigated the influence of various process parameters on the multi-layer deposition of laser-melted Inconel® 625 powder in a process analogous to both laser cladding and $LENS_U$. Their study examined a range of parameters — including laser irradiance, stage translation velocity, powder mass flow rate, powder particle size distribution, and the Z-directional incremental step between successive layers

— and quantified their respective effects on the size of the heat-affected zone (HAZ) generated during the deposition process. The HAZ was operationally defined as the region of the substrate that undergoes melting below the deposition surface and was characterized through post-build metallographic examination.

Khalen and Kar [10] conducted a systematic investigation into the effects of multiple process parameters on the tensile yield strength of AISI 304 stainless steel thin plates deposited via a process functionally identical to $LENS_U$, referred to as Laser-Aided Direct Rapid Manufacturing (LADRM). Their objective was to establish a range of admissible input parameter values within which deposited components would exhibit mechanically acceptable properties. The analytical methodology employed the Buckingham Π-Theorem to express the relevant heat transfer and powder mass flux process variables as a set of 14 dimensionless governing parameters.

Rangaswamy et al. [11, 12] pursued an experimental characterization of residual stress fields in $LENS_U$-deposited structures using the neutron diffraction technique. Their measurements were performed on $LENS_U$- produced rectangular plates of AISI 316 stainless steel. Neutron diffraction data were systematically collected at numerous spatially distributed points throughout the sample volume to construct a comprehensive map of the internal stress state. The axial components of residual stress were subsequently computed via Hooke's law and plotted as a function of spatial position within the plate — first along the height (Z- direction) at the vertical centreline, and then along the width (Y-direction) at the horizontal mid-plane.

Wang and Felicelli [15] conducted a parametric study conceptually analogous to that performed by Hofmeister et al. [8], with the objective of determining whether consistent trends in cooling rates and thermal gradients were reproducible across different levels of laser power. By repeating the baseline simulation at five distinct power intensity values, they demonstrated that the thermal gradient at the boundary of the molten pool increases considerably with laser power, whereas the associated cooling rate exhibits a corresponding decrease.

Neela and De [16] employed the general- purpose finite element package ABAQUS®

6.6 to investigate the effects of scanning speed and laser power on the resulting temperature distribution. Their model incorporated an element activation/deactivation scheme consistent with prior studies, and simulated the deposition of a thin plate of AISI 316 stainless steel with temperature-dependent thermal conductivity and specific heat defined by linear and quadratic relationships, respectively.

Deus and Mazumder [17] developed a thermomechanical finite element model to predict the residual stress state resulting from laser cladding of C95600 copper alloy deposited onto an AA333 aluminium alloy substrate. Since residual stresses in this configuration arise primarily from the differential thermal expansion of the dissimilar deposited and substrate materials, accurate stress prediction was contingent upon reliable reconstruction of the transient temperature fields produced during fabrication.

Labudovic et al. [18] developed a three- dimensional coupled thermomechanical model for the simulation of direct laser metal powder deposition — a process operationally equivalent to $LENS_U$ — using the ANSYS® finite element platform. Their model simulated the deposition of a 50 mm × 20 mm × 10 mm thin plate of MONEL 400 onto an AISI 1006 steel substrate, employing the ANSYS® element activation option to replicate the progressive material addition. The laser energy input density was represented as a spatially moving Gaussian distribution, implemented through the ANSYS® Parametric Design Language (APDL). The constitutive behaviour was governed by a temperature-dependent visco- plastic formulation in which viscous contributions were neglected.

3. THERMAL MODELLING

3.1 Temperature Distribution

In the $LENS_U$ process, the interaction of a traversing laser beam with the substrate induces localized melting of both the deposited powder and a portion of the underlying substrate material. Upon removal of the laser source, the molten region undergoes rapid solidification. The transient temperature field within the substrate can be determined by solving the three-dimensional heat conduction equation:

$$\partial/\partial x\,(k\,\partial T/\partial x) + \partial/\partial y\,(k\,\partial T/\partial y) + \partial/\partial z\,(k\,\partial T/\partial z) = \rho\, c_p\,(\partial T/\partial t) \quad \dots (1)$$

where k denotes the thermal conductivity, T is the temperature, ρ is the material density, c_p is the specific heat capacity, and t is time. The left-hand side of Eq. (1) represents the conductive heat flux within the domain, while the right-hand side accounts for the transient thermal energy storage at any given point. The following boundary conditions are imposed:

The prescribed heat flux is defined as the power density of the laser beam. Assuming a spatially uniform laser beam intensity distribution:

$$Q(x, y, z, t) = Pa / (\pi\, r_0^2) \quad \dots (2)$$

where P is the laser power, a is the absorptivity of the deposited material, and r_0 is the effective laser beam radius. The thermal boundary conditions governing convective and radiative heat exchange at the exposed surfaces are expressed as:

$$\text{Convection: } -k\,\nabla T = h(T - T_0) \quad \dots (3)$$

$$\text{Radiation: } -k\,\nabla T = \varepsilon\sigma(T^4 - T_0^4) \quad \dots (4)$$

where h is the convective heat transfer coefficient, ε is the surface emissivity, σ is the Stefan–Boltzmann constant, and T_0 is the ambient reference temperature. The initial thermal condition is given by:

$$T(x, y, z, 0) = T_0 \quad \text{and} \quad T(x, y, z, \infty) = T_0 \quad \dots (5)$$

3.2 Stress Analysis

In the present formulation, no externally applied body forces or surface tractions are considered; the sole mechanical load acting on the system is the transient thermal field. The pronounced temperature gradients generated by the laser beam induce thermal strains of sufficient magnitude to cause localized plastic yielding of the workpiece material. The total strain tensor is decomposed as:

$$\varepsilon_{ij} = \varepsilon_{ij}^{e} + \varepsilon_{ij}^{j} + \varepsilon_{ij}^{th} \quad \dots (6)$$

where the superscripts e, p, and th denote the elastic, plastic, and thermal components of strain, respectively. The elastic and thermal strain components are expressed as:

$$\varepsilon_{ij}^{e} = [(1+\nu)/E]\,\sigma_{ij} - [\nu/E]\,\sigma_{kk}\,\delta_{ij} \quad \dots$$

$$(7)\ \varepsilon_{ij}^{th} = \alpha(T - T_0)\delta_{ij} \quad \dots (8)$$

where E is Young's modulus, ν is Poisson's ratio, α is the coefficient of thermal expansion, and δ_{ij} is the Kronecker delta. To evaluate the plastic strain component, a kinematic hardening model in conjunction with the von Mises yield criterion is adopted.

3.3 Modelling Assumptions

The following simplifying assumptions are adopted in the thermal and structural simulation of the $LENS_U$ process:

The substrate is assumed to be at uniform ambient temperature (20°C) at the commencement of the deposition process. The thermal boundary condition applied to the substrate periphery is convective heat transfer with a spatially uniform and temporally constant coefficient. The laser heat flux is treated as a moving source with a uniform distribution applied exclusively to the currently active (deposited) elements. The activated elements within the molten pool region are initialized at the material melting temperature. Convective heat redistribution within the molten pool is accounted for in the model. The substrate is assumed to be in a stress-free state at the outset of the process, positioned freely on the worktable without any clamping constraints to restrict its in-plane deformation. The laser scanning velocity is treated as constant, and the dwell time associated with direction changes between successive scan tracks is taken as 4 seconds. The progressive addition of powder material onto the substrate is discretized into numerous small time increments to capture the quasi-steady-state nature of the $LENS_U$ process.

3.4 Transient Thermal Analysis

Thermal conductivity and specific heat capacity are both treated as temperature- dependent material properties. The heat transfer mechanism considered in the model is predominantly conduction; convective effects within the melt pool are partially incorporated, while radiation is excluded. The latent heat associated with the solid-to- liquid phase transformation of SS 304 is explicitly accounted for in the formulation. The element birth and death technique available in ANSYS is employed to simulate the sequential addition of new material elements to the computational domain, corresponding to the layer-by-layer deposition of powder during multi-layer fabrication. The substrate is modelled as a passive thermal sink. The Boolean operations in ANSYS are utilized to ensure continuous material bonding between the substrate and successive deposition layers. Temperature-dependent thermal and mechanical properties of SS 304 are assigned to both the thin wall and substrate domains.

3.5 Finite Element Model

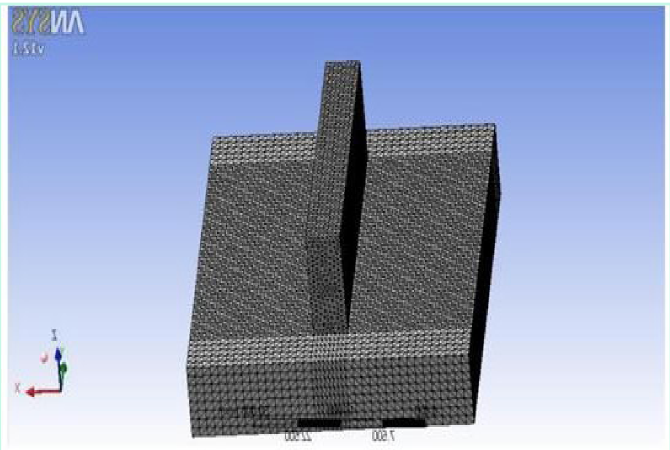

A dedicated finite element model of the $LENS_U$ process was developed for the present investigation. The substrate dimensions are 40 mm × 40 mm × 10 mm. The thin-walled structure under analysis has a length of L = 30 mm, a width of W = 6 mm, and a height of H = 14 mm. Six tracks spanning the width are assumed, each of uniform 1 mm width, while the wall height comprises 20 uniformly spaced deposition layers, each of 0.7 mm thickness. Each individual layer therefore measures 30 mm in length, 1 mm in width, and 0.7 mm in height.

As illustrated in Figure 2, the discretized model consists of 25,402 nodes and 14,951 tetrahedral elements. The laser beam transit time for a single scan pass is 4 seconds, subdivided into 20 equal time increments of 0.20 seconds each. An additional cooling time step of t = 200 s is appended after the final deposition pass to simulate the post- deposition thermal relaxation of the structure.

4. MODELLING CONSIDERATIONS

4.1 Thermal Boundary and Initial Conditions

The substrate is initialized at ambient temperature at the start of the simulation, with T_0 = 20°C = 293 K. Convective heat transfer with a constant coefficient of 30 W/m²K is applied to the lateral and upper surfaces of the substrate. The effective convection coefficient applied to the bottom surface of the substrate — which interfaces with the worktable — is 400 W/m²K. Temperature-dependent material properties are applied in a stepwise manner as specified in Table 1.

Table 1: Temperature-Dependent Thermomechanical Properties of AISI 304 Stainless Steel

Temperature T (°C)	Thermal Conductivity ($W·m^{-1}·K^{-1}$)	Yield Stress σY (MPa)	Young's Modulus E (GPa)	Latent Heat of Fusion (J/kg)
25	14.8	241	193	—
400	20.7	159	—	—
600	23.5	134	—	—
800	25.8	114	—	—
1000	28.8	97	—	—
1100	29.9	—	—	—
1200	31.6	88	—	—
1300	32.8	76	—	—
1454	—	—	—	2.65×10^5

4.2 Structural Boundary and Initial Conditions

The substrate is assumed to be entirely free of residual stress at the commencement of the simulation. The sole external load applied to the structural model is the thermal field derived from the preceding thermal analysis. Displacement boundary conditions are imposed on the bottom face of the substrate to prevent rigid-body motion in the Z- direction, while the substrate remains unconstrained and free to deform in the X and Y directions.

5. SIMULATION RESULTS

5.1 Temperature Distribution

In practice, the $LENS_U$ fabrication process involves multi-track, multi-layer deposition sequences. In the present simulation, a laser power of 3.0 kW, a scanning rate of 14 mm s^{-1}, and a powder delivery rate of 0.002 kg s^{-1} are prescribed. Following the completion of the final deposition step, the simulated temperature field exhibits a maximum temperature of 2,038.77 K, with a minimum recorded temperature of 20.00 K. The temperature undergoes a rapid transient decay immediately after the laser source is deactivated. The instantaneous temperature at any point within the domain attains its peak value precisely as the laser beam traverses over that location, after which the temperature declines sharply in accordance with the prevailing conductive cooling conditions. The maximum temperature recorded immediately after laser deactivation falls appreciably below the material's melting threshold.

6. RESULTS AND DISCUSSION

Table 2: Summary of Stress and Deformation Results Across All Deposition Configurations (5, 10, 15, and 20 Layers)

Mechanical Parameter	Extreme Value	Location
Von Mises Stress — Maximum	Maximum	Substrate
Von Mises Stress — Minimum	Minimum	Thin Wall
Shear Stress — Maximum	Maximum	Substrate
Shear Stress — Minimum	Minimum	Thin Wall
Total Deformation — Maximum	Maximum	Substrate
Total Deformation — Minimum	Minimum	Thin Wall

The thermal analysis confirms that the progressive addition of deposition layers exerts a direct influence on the temporal temperature history of the process. The non- uniform distribution of the thermal field constitutes a primary contributing factor to the development of internal stresses within

the deposited structure. Figure 7 presents the von Mises stress distribution at the conclusion of the deposition process for each layering configuration, together with the maximum von Mises stress values recorded across the various layer counts. Across all deposition patterns examined, the peak stress consistently manifests at the interface between the deposited material and the substrate.

To facilitate a more detailed assessment of the stress state within the deposited material, the von Mises stress distribution at the surface of the deposited structure is presented in the accompanying figures. As demonstrated in Figure 8, the maximum shear stress increases monotonically with the number of deposited layers. Conversely, as illustrated in Figure 9, the total deformation exhibits a non-monotonic behaviour — initially decreasing before subsequently increasing — attributable to the influence of the deposition sequencing strategy and the transient effects associated with the applied power.

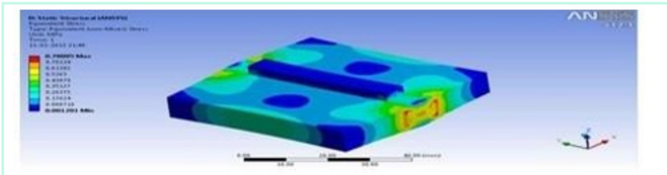

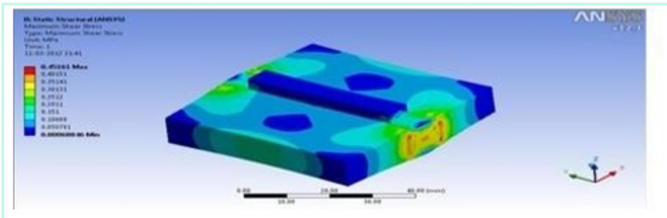

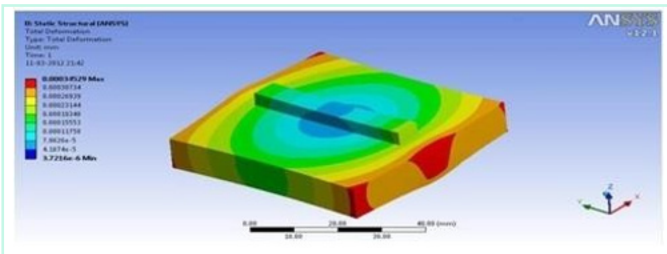

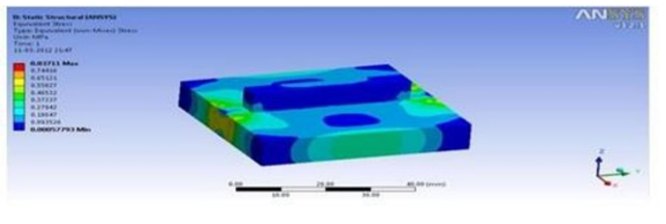

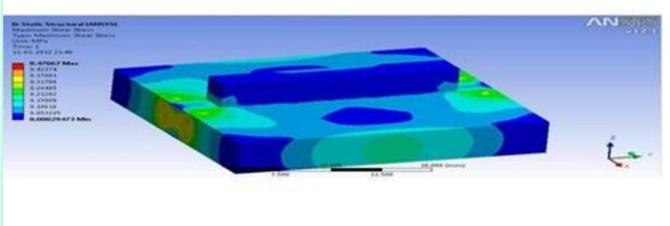

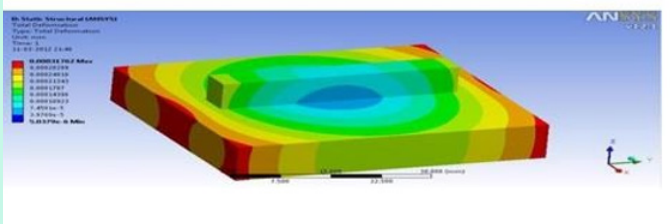

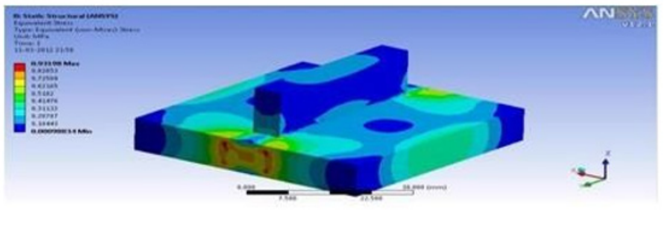

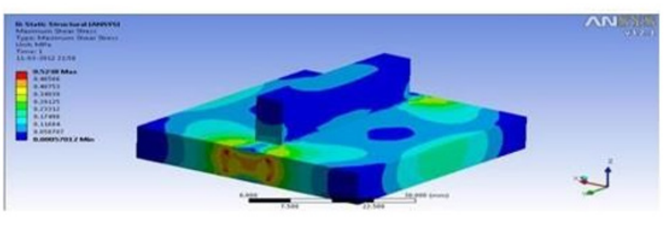

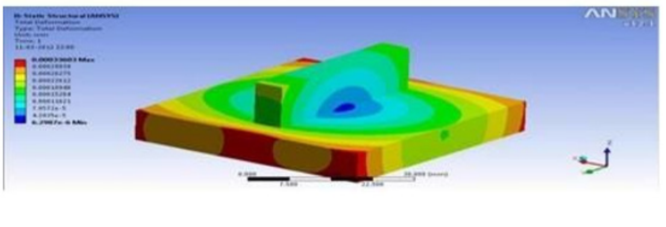

Results and discussion

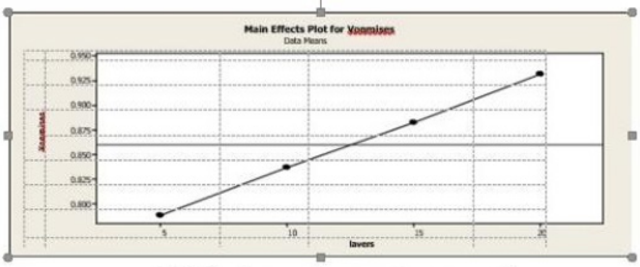

Relation between layers and max. von-mises stress

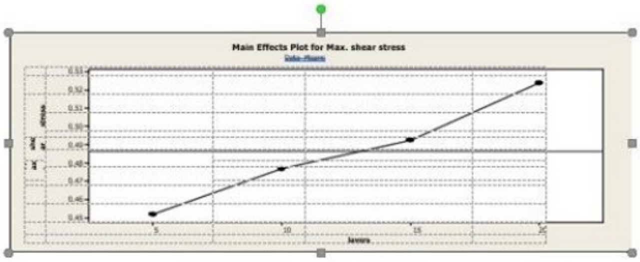

Relation between layers and max. shear stress

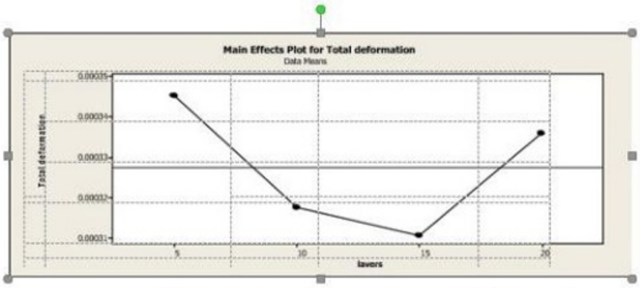

Relation between layers and max. total deformation

		Location
Von-mises	Maximum	Substrate
	Minimum	Thin wall
Shear stress	Maximum	Substrate
	Minimum	Thin wall
Total deformation	Maximum	Substrate
	Minimum	Thin wall

6. CONCLUSION

Despite the variation in activation timing across successive deposition layers, all layers exhibit broadly consistent trends in temperature evolution and thermally induced stress development. The dominant thermal gradients within the deposited specimen are oriented primarily in the Z-direction (through-thickness). Among all components of the von Mises effective stress, the Z- directional thermal stress component is substantially larger than its in-plane counterparts.

In successive deposition layers, the von Mises effective stress, total deformation, and shear stress values in each newly deposited layer are approximately double those of the immediately preceding layer. The initiation point of each deposition pass exerts a pronounced influence on both the spatial distribution and the intensity of the resulting thermal stress field. During the $LENS_U$ process, elevated thermal gradients preferentially develop in the through-thickness direction. The consequent differential thermal contraction generates considerable internal stresses, which are sufficient to induce plastic yielding in the thermally softened near-surface regions. The present investigation has demonstrated that the peak temperature at any given location is attained precisely as the laser beam passes over that point. Upon departure of the laser beam, the freshly deposited metallic material undergoes rapid solidification with an extremely high initial cooling rate that diminishes progressively with time.

During the deposition of subsequent layers, the temperature at previously solidified locations is periodically elevated as the laser beam traverses analogous positions in overlying layers, thereby generating repetitive thermal cycling. These cyclic thermal events are directly correlated with the progressive accumulation of total deformation, von Mises stress, and shear stress observed throughout the build sequence.

7. ACKNOWLEDGEMENTS

The authors wish to express their sincere gratitude and profound appreciation to Prof. R. I. Patel for his exceptional guidance, insightful suggestions, and constructive critical evaluation throughout the course of this investigation. The first author considers it a privilege to have conducted this research under the supervision of such a distinguished academic. The authors also extend their appreciation to Mr. A. H. Makwana for his invaluable cooperation and support throughout the duration of this study.

REFERENCES

1. Vilar, R. J. (1999). Laser Cladding. Journal of Laser Applications, 11(2), 64–79.
2. Atwood, C., Griffith, M., Harwell, D., Reckaway, D., Ensz, M., Keicher, D., Schlienger, M., Romero, M., Oliver, M., Jeanette, F., & Smugeresky, J. (1999). Laser Spray Fabrication for Net-Shape Rapid Product Realization LDRD. Sandia National Laboratories Technical Report.
3. Sandia National Laboratories. Official Website. www.sandia.gov
4. Griffith, M., Ensz, M., Puskar, J., Robino, C., Brooks, J., Philliber, J., Smurgeresky, J., & Hofmeister, W. (2000). Understanding the Microstructures and Properties of Components Fabricated by Laser Engineered Net Shaping (LENS). Materials Research Society Symposium Proceedings, Vol. 625, pp. 9–21.
5. Keicher, D., Jellison, J., Schanwald, L., & Romero, J. (1995). Towards a Reliable Laser Spray Powder Deposition System through Process Characterization. Proceedings of the 27th International Technical Conference, Society for the Advancement of Material and Process Engineering, Albuquerque, NM, pp. 1009–1018.
6. Hofmeister, W., Wert, M., Smurgeresky, J., Philliber, J., Griffith, M., & Ensz, M. Investigating Solidification with the Laser Engineered Net Shaping ($LENS_U$) Process. JOM-e.
7. Hofmeister, W., Griffith, M., Ensz, M., & Smurgeresky, J. (2001). Solidification in Direct Metal Deposition by LENS Processing. JOM, 53(9), 30–34.
8. Hofmeister, W., MacCalum, D., & Knorovsky, G. (1998). Video Monitoring and Control of the LENS Process. Proceedings of the American Welding Society 9th International Conference on Computer Technology in Welding, Detroit, MI, pp. 187–196.
9. Smugeresky, J., Keicher, D., Romero, J., Griffith, M., & Harwell, L. (1997). Laser Engineered Net Shaping ($LENS_U$) Process: Optimization of Surface Finish and Microstructural Properties. Proceedings of the World Congress on Powder Metallurgy and Particulate Materials, Princeton, NJ, Part 21.
10. Kahlen, F.-J., & Kar, A. J. (2001). Tensile Strengths for Laser-Fabricated Parts and Similarity Parameters for Rapid Manufacturing. Journal of Manufacturing Science and Engineering, 123(1), 38–44.
11. Rangaswamy, P., Holden, T., Rogge, R., & Griffith, L. J. (2003). Residual Stresses in Components Formed by the Laser Engineered Net Shaping (LENS®) Process. Journal of Strain Analysis for Engineering Design, 38(6), 519–528.
12. Rangaswamy, P., Griffith, M., Prime, M., Holden, T., Rogge, R., Edwards, J., & Sebring, R. (2005). Residual Stresses in LENS® Components Using Neutron Diffraction and the Contour Method. Materials Science and Engineering A, 399, 72–83.
13. Riqing, Y., Smugeresky, J., Zheng, B., Zhou, Y., & Lavernia, E. (2006). Numerical Modelling of the Thermal Behaviour during the LENS® Process. Materials Science and Engineering A, 428, 47–53.
14. Lindgren, L.-E. (2001). Finite Element Modelling and Simulation of Welding — Part 3: Increased Complexity. Journal of Thermal Stresses, 24, 195–231.
15. Wang, L., & Felicelli, S. (2006). Analysis of Thermal Phenomena in $LENS_U$ Deposition. Materials Science and Engineering A, 435–436, 625–631.
16. Neela, V., & De, A. (2007). Numerical Modelling of $LENS_U$ Process Using Special Element Features. Proceedings of the 2007 Abaqus India Regional Users' Meeting.
17. Deus, A., & Mazumder, J. (1996). Two- Dimensional Thermo-Mechanical Finite Element Model for Laser Cladding. Proceedings of ICALEO, Orlando, FL: Laser Institute of America, pp. B/174–B/183.
18. Labudovic, M., Hu, D., & Kovacevic, R. (2003). A Three-Dimensional Model for Direct Laser Metal Powder Deposition and Rapid Prototyping. Journal of Materials Science, 38, 35–49.